Journal of Environmental Chemical Engineering 4 (2016) 3882–3890

Contents lists available at ScienceDirect

Journal of Environmental Chemical Engineering

journal homepage: www.elsevier.com/locate/jece

Magnetic nickel ferrite nanoparticles for removal of dipyrone from aqueous solutions

Valeria Springer*, Eliana Pecini, Marcelo Avena

INQUISUR (CONICET-UNS), Departamento de Química, Universidad Nacional del Sur, Av. Alem 1253, B8000CPB Bahía Blanca, Argentina

ARTICLE INFO

Article history:
Received 28 April 2016
Received in revised form 11 August 2016
Accepted 27 August 2016
Available online 30 August 2016

Keywords:
Adsorption
Emerging pollutants
Nickel ferrite nanoparticles
Pharmaceuticals

ABSTRACT

Magnetic nickel ferrite nanoparticles with a size of 20 ± 3 nm have been synthesized by a co-precipitation method at room temperature. Crystalline structured particles with ferromagnetic properties were obtained by calcination at 600 °C. These nanoparticles were characterized in order to determine the particle size distribution, morphology, surface charge and adsorption properties. Nickel ferrite nanoparticles were tested as potential adsorbent for removal of dipyrone from aqueous solution by evaluating adsorption kinetics and isotherms. The maximum adsorption capacities at 20 °C were 30.4 mg g^{-1} (pH 6) and 25.0 mg g^{-1} (pH 4). Additionally, analytical solution of the Langmuir adsorption kinetic equation was successfully applied. Desorption experiments were conducted at lab scale by using a flow through system aiming to study the release of dipyrone from the proposed material at different experimental conditions. A 55% of desorption for pre-sorbed DIP is achieved by performing several extraction cycles with an aqueous solution (pH 2.5) at 50 °C. Also, 43% desorption was obtained by adding 0.2 M phosphate, and 48% by adding 0.2 M sulfate. With the advantages of low cost and rapid processing, these magnetic nanoparticles could gain a promising application in the removal of pharmaceutical compound residues during treatment of water samples on a large scale.

1. Introduction

The occurrence of pharmaceuticals and related compounds in the aquatic environment has been recognized as an emerging problem. The continuous discharge of pharmaceuticals into the environment results in a prolonged exposure of aquatic organisms and animals to these compounds and/or their active metabolites [1,2]. In this concern, compounds such as antibiotics, antidepressants, estrogens and analgesics are the most commonly found in wastewater and environmental water [3,4]. Dipyrone is a common analgesic, antispasmodic and antipyretic drug, especially used in clinical treatments, that has been banned in some countries due to its potential association with diseases such as agranulocytosis [5]. Nevertheless, this compound is one the most consumed pharmaceuticals in Argentina, Brazil, Germany, Italy and Spain, among others [6]. Additionally, dipyrone is used in veterinary practices for domestic and farm animals, such as horses and cattle, so this compound is under scope of the European Regulation [7]. Recently, dipyrone residues were found in water samples, as a consequence of its high solubility in water and its high polarity [6,8].

Adsorption processes are widely applied to remove organic pollutants from aqueous media, including drinking water, wastewater, groundwater and surface water. Several adsorbents such as carbon-based materials and synthetic resins have been investigated for adsorption of pharmaceutical compounds [9]. However, extensive application of some of these adsorbents is limited due to the high cost, difficult disposal and regeneration. In this concern, the use of magnetic nanoparticles represents an interesting and economical alternative due to their simple synthesis and manipulation [10]. Synthesis of nanoscale ferrites (represented by the general formula MFe_2O_4, where M is usually a divalent metal ion) commonly implies co-precipitation, solvo/hydrothermal and microemulsions routes [11,12]. Among these, the co-precipitation method is widely used because of its simplicity, low cost, rather low synthesis temperature and small particle size obtained. Although ferrites are used in applications such as inductors, transformers, gas sensors [13], photocatalyst [14] and adsorbent for removal of dyes [15], these nanosized magnetic particles are being also considered as potential adsorbents of pharmaceutical compounds due to their high surface area and the advantage of separation under application of magnetic fields and regeneration by heating at high temperatures. As an example, magnetite (Fe_3O_4 or, more explicitly, $Fe^{II}Fe^{III}{}_2O_4$) particles have been applied for

* Corresponding author.
E-mail address: valeria.springer@uns.edu.ar (V. Springer).

http://dx.doi.org/10.1016/j.jece.2016.08.026
2213-3437/

extraction of tetracycline and sulfonamide compounds in aqueous solution [16,17]. Particularly, nickel ferrite ($NiFe_2O_4$), which has an inverse spinel cubic structure where Fe^{3+} ions are located at the tetrahedral sites while octahedral sites are occupied by Fe^{3+} and Ni^{2+} ions, is a soft magnetic material with low saturation magnetization but high electrical resistivity. This material has been recently used as adsorbent for removal and degradation of organic dyes [18,19]. Nevertheless, there are no experimental studies presented in the literature where nickel ferrite particles are proposed for adsorptive removal of pharmaceutical compounds.

In this work, synthesized nickel ferrite nanoparticles (NFNPs) are proposed for removal of dipyrone (DIP) in aqueous solution. The adsorption process was studied by analyzing adsorption kinetics and isotherms under various experimental conditions to evaluate the potential effects of the surface charge, pH and temperature on the adsorption capacity. Adsorption and desorption rate constants were obtained by solving the Integrated Kinetic Langmuir equation, (IKL). In addition, desorption studies were performed aiming to evaluate the release of DIP from the adsorbent material. For this purpose, a flow system was implemented for evaluating desorption processes under different conditions of pH and temperature with minimal handling of samples and reagents.

2. Materials and methods

2.1. Chemicals

Ferric chloride hexahydrate ($FeCl_3{\cdot}6H_2O$, 97%) was obtained from Anedra (Argentina) and nickel chloride hexahydrate ($NiCl_2{\cdot}6H_2O$) was purchased from Biopack (Argentina). Sodium hydroxide was obtained from Merck (Germany). Hydrochloride acid, sodium chloride, sodium hydrogen phosphate, sodium bicarbonate and sodium sulfate were purchased from Cicarelli (Argentina). Dipyrone (DIP, chemical formula $C_{13}H_{16}N_3NaO_4S$) was obtained from Parafarm (Argentina). All chemicals were of analytical grade and used as received. Ultrapure water (18 MΩ cm^{-1}) was used for the preparation of solutions. Stock solutions of DIP and aqueous dilutions were stored in darkness to prevent degradation.

2.2. Synthesis of nano sized nickel ferrite

A co-precipitation method was used for the synthesis of nanocrystalline powder $NiFe_2O_4$. Ferric chloride and nickel chloride aqueous solutions were mixed in a 1:2 molar ratio with constant stirring. Then, a 2.0 M NaOH solution was added dropwise (1.0 mL min^{-1}) to the above solution while monitoring the pH. The co-precipitation reaction was carried out at room temperature (23 °C ± 2 °C) and a brown colored precipitate was obtained at pH 11.4. The precipitate was washed several times with distilled water until the pH of the slurry became 6 and the conductivity 272 μS cm^{-1}. The wet slurry was dried at 105 °C for 4 h and then it was grounded and subjected to calcination at 600 °C for 5 h.

2.3. Characterization

The powder was characterized at several stages using X-ray diffraction (XRD). XRD patterns were obtained with a Philips PW 1710 diffractometer with CuKα radiation (λ = 1.54059 Å) and a graphite monochromator operated at 45 kV, 30 mA and 25 °C at a scan rate of 2θ s^{-1}. The N_2-BET method was employed for surface area, pore volume and pore diameter determination. The N_2 adsorption isotherms at 77.4 K were measured with a Quantachrome Nova 1200e instrument. Thermogravimetric analyses were run from 20 to 800 °C at a heating rate of 5 °C min^{-1} with a Rigaku Thermoflex TG 8110 equipment. The IR spectra were measured in the 400–4000 cm^{-1} region (2 cm^{-1} resolution) to samples dispersed in KBr discs. All spectra were recorded with a Nicolet FT-IR Nexus 470 Spectrophotometer.

The magnetic properties were measured on a VSM-7404 vibrating sample magnetometer (VSM) with a maximum magnetic field applied of 1900 Oe at room temperature. A defined amount (42.98 mg ± 1.43 mg) of the synthesized sample dried at room temperature, 40 °C, 75 °C, 105 °C and calcined at 600 °C was taken and subjected to analysis.

TEM analysis was performed using a JEOL 100 CX II transmission electron microscope, operated at 100 kV with magnification of 450,000x. Observations were made in a bright field.

The electrophoretic mobility of synthesized NFNPs was measured with a Zetasizer Nano ZS90 instrument (Malvern Instruments Ltd.) at 25 °C and the zeta potential was calculated using the Smoluchowski equation [20]. Stock suspensions of nickel ferrite (200 mg L^{-1}) in 0.01 M NaCl as supporting electrolyte were subjected to analysis using 0.1 M HCl and 0.1 M NaOH solutions to adjust the pH of suspensions. In order to evaluate the surface charge on NFNPs after adsorption of DIP in aqueous solution, electrophoretic mobility measurements were performed in the pH range of 2.5–9.5 for the following initial concentrations of DIP: 3, 30 and 200 mg L^{-1}, including 0.01 M of NaCl as supporting electrolyte. Samples were equilibrated for 30 min before analysis.

2.4. Batch adsorption experiments

DIP, which contains a sulfonic group in the molecule (Table 1), is fully dissociated at pH values above 2.0 [21], thus adsorption experiments were performed in the pH range 2.5–9.5.

DIP adsorption isotherms were carried out using polypropylene tubes covered with polypropylene caps. Each tube contained 8 mg of NFNPs, the desired volume (from 0 to 500 μL) of a 4 g L^{-1} stock DIP solution to cover a concentration range from 0 to 200 mg L^{-1} and the needed volumes of 0.1 M NaCl solution to achieve a final

Table 1
Physicochemical properties of dipyrone [Ref. [21]].

Physicochemical properties	Dipyrone structure
Molar mass: 333.34 g mol^{-1} logP: −0.82 Solubility at 25 °C: very soluble in water, soluble in ethanol and methanol, practically insoluble in methylene chloride	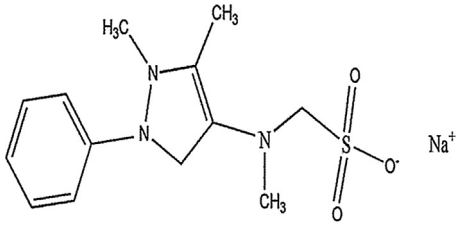

NaCl concentration of 0.01 M. The pH of the so-prepared dispersions was then adjusted by adding small volumes (microliters) of 0.1 M HCl or NaOH and ultrapure water was added to a final total volume of 10 mL. After equilibration, the solid and liquid phases were separated employing a Nd magnet and different aliquots were taken to quantify the DIP concentration that remained in the liquid phase (supernatant).

The uptake of DIP by the NFNPs was calculated as follow:

$$a_{eq} = \frac{c_o - c_{eq}}{m} V \quad (1)$$

where a_{eq} is the uptake after equilibration (mg g^{-1}), c_o and c_{eq} (mg L^{-1}) are respectively the initial and equilibrium concentrations of DIP in the aqueous solution, V is the total volume (L) and m is the amount of NFNPs (g).

Two kinetic runs, one at pH 4 and the other one at pH 6 were also performed in order to check the effect of time on adsorption. The procedure was similar to that described above, but instead of waiting for equilibration, the supernatants were analyzed as a function of the adsorption time during 420 min.

2.5. Desorption experiments

In order to evaluate the possible release of DIP from the NFNPs, desorption experiments were carried out at different pH and temperatures. A flow system composed by a peristaltic pump, an extraction syringe and a mixing cell was adapted to perform the washing cycles, which were done by mixing DIP-loaded NFNPs with 14 mL of extraction solution with constant stirring and controlled temperature. Briefly, a 10 mL aqueous mixture of 800 mg L^{-1} NFNPs and 100 mg L^{-1} DIP in 0.01 M NaCl at pH 6.0 was delivered by a peristaltic pump to a mixing cell with continuous stirring to produce the DIP adsorption. After agitation for 60 min, the nanoparticles were magnetically decanted and aliquots were withdrawn with the extraction syringe for DIP quantification. Then, the supernatants were delivered to the waste reservoir and the adsorbent was rinsed with water to remove any excess of DIP. A 14 mL of extraction solvent was pumped into the system and mixed with the DIP-loaded NFNPs while maintaining constant stirring. Temperature was controlled by using a thermostatized bath. After the contact time, the stirring was discontinued and nanoparticles were magnetically separated. A 2 mL aliquot of the supernatant was withdrawn and diluted to 4 mL prior to DIP quantification.

2.6. Quantification process

For quantification of DIP two spectrophotometric methods were proposed on the literature [22,23]. In the first method (Method no. 1) DIP was determined through the reaction between dipyrone and ammonium molybdate in acidic medium at 60 °C to produce blue molybdenum, which is detected spectrophotometrically at 620 nm. Method no. 2 is based on the hydrolysis of DIP under acid conditions and detection at 258 nm. As can be seen in Table S1 (Supplementary material), DIP can be quantified employing both methods at the studied concentration range. Nevertheless, method no. 2 was selected for further application due to its sensibility, simplicity and the short time consumed for analysis. The whole procedure was applied as follow: A calibration curve between 1 and 100 mg L^{-1} was constructed by preparing the standard solutions in 0.1 M HCl and absorbance data was recorded at 258 nm with an Agilent 8453 diode array spectrophotometer using a 1-cm quartz cell. The calibration curve was $Y = (0.0252 \pm 0.0007)X + (0.0134 \pm 0.0086)$ with $R^2 = 0.9994$. For analysis of supernatants, a 1:2 dilution in 0.1 M HCl was made prior to analysis.

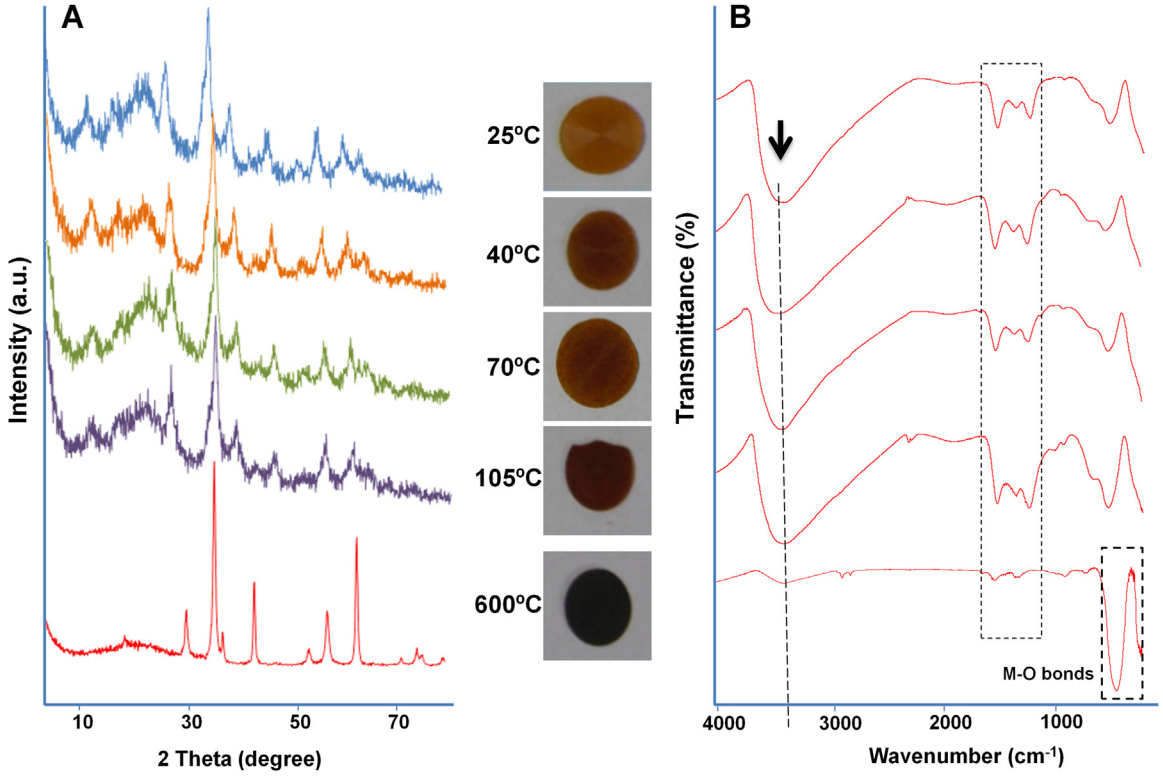

Fig. 1. Characterization of the synthesized samples by: (A) XRD and (B) infrared spectroscopy. From the top to the bottom: samples dried at 25 °C, 40 °C, 70 °C, 105 °C and calcined at 600 °C. Inset: changes in color during drying and calcination processes.

3. Results and discussion

3.1. General characteristics of the synthesized nickel ferrite

Fig. 1 shows XRD patterns and IR spectra of the solid synthesized by the co-precipitation method after drying at different temperatures and after calcination at 600 °C. The figure also presents the pictures of the different solids in the dry state to visualize how the samples look like with the naked eye. Samples dried up to 105 °C show a XRD pattern that corresponds to a poorly crystalline material, which already has the main reflections that correspond to nickel ferrite. The calcination at 600 °C results in a highly crystallized and pure nickel ferrite. There is no evidence of the presence of other iron oxides or nickel oxide phases, in agreement with previous results in the literature [24]. The diffraction peaks can be indexed to a face centered cubic structure of nickel ferrite and the crystallite size (D_{311}) was estimated to be 16.6 nm using the Scherrer's equation [25]. This size is comparable to data reported in the literature for nickel ferrite particles obtained by calcination process at 600 °C [26]. The IR spectra show strong and broad bands at 3416 cm^{-1} and 1635 cm^{-1} for samples dried between 25 and 105 °C, attributed to the O—H stretching and vibration modes of adsorbed water. Additionally, two bands in the region of 1370–1450 cm^{-1} can be assigned to the asymmetric stretching mode of adsorbed carbonate groups [27]. Regarding the calcined sample, the two main bands between 604 and 400 cm^{-1} observed in the spectrum correspond to the metal–oxygen vibration bands in the crystal lattices. These bands could be assigned to the intrinsic stretching vibrations of Fe-O and Ni-O in the spinel structure, respectively [28]. No other bands, which could be assigned to other nickel and iron oxides phases were detected in the spectrum of calcined samples [29,30]. Additionally, it is possible to appreciate changes in color by the naked eye during the drying and calcination processes of NFNPs, which can be associated with the evaporation of structural water and crystallization process.

Fig. 2 shows the TEM micrographs and results from the magnetic characterization of the studied NFNPs. Most of the particles appear polyhedral in shape, with a particle size of 20 ± 3 nm (average ± standard deviation, n = 40). This is a value close to the estimated using XRD. Even though it is recognized that the Scherrer equation may sometimes misjudge the nanoparticle size [31], it works rather well for the solid studied here. The magnetic hysteresis curve of the calcined sample showed saturation magnetization (Ms = 26 emu g^{-1}), remanent magnetization (Mr = 2.7 emu g^{-1}) and coercivity (Hc = 95 Oe), exhibiting ferromagnetic behavior. The value of Ms resulted small compared to that of bulk nickel ferrite (55 emu g^{-1}) [32]. All the other samples resulted paramagnetic, indicating that the ferromagnetic behavior is only achieved after calcination (Fig. S1).

From the nitrogen adsorption/desorption isotherms, the BET surface area and average pore volume were calculated as 36.91 $m^2 g^{-1}$ and 0.33 $cm^3 g^{-1}$, respectively (Fig. S2).

Thermogravimetric analyses showed a significant weight loss from 20 °C to 250 °C for samples dried at room temperature, which is probably attributed to moisture evaporation and loss of

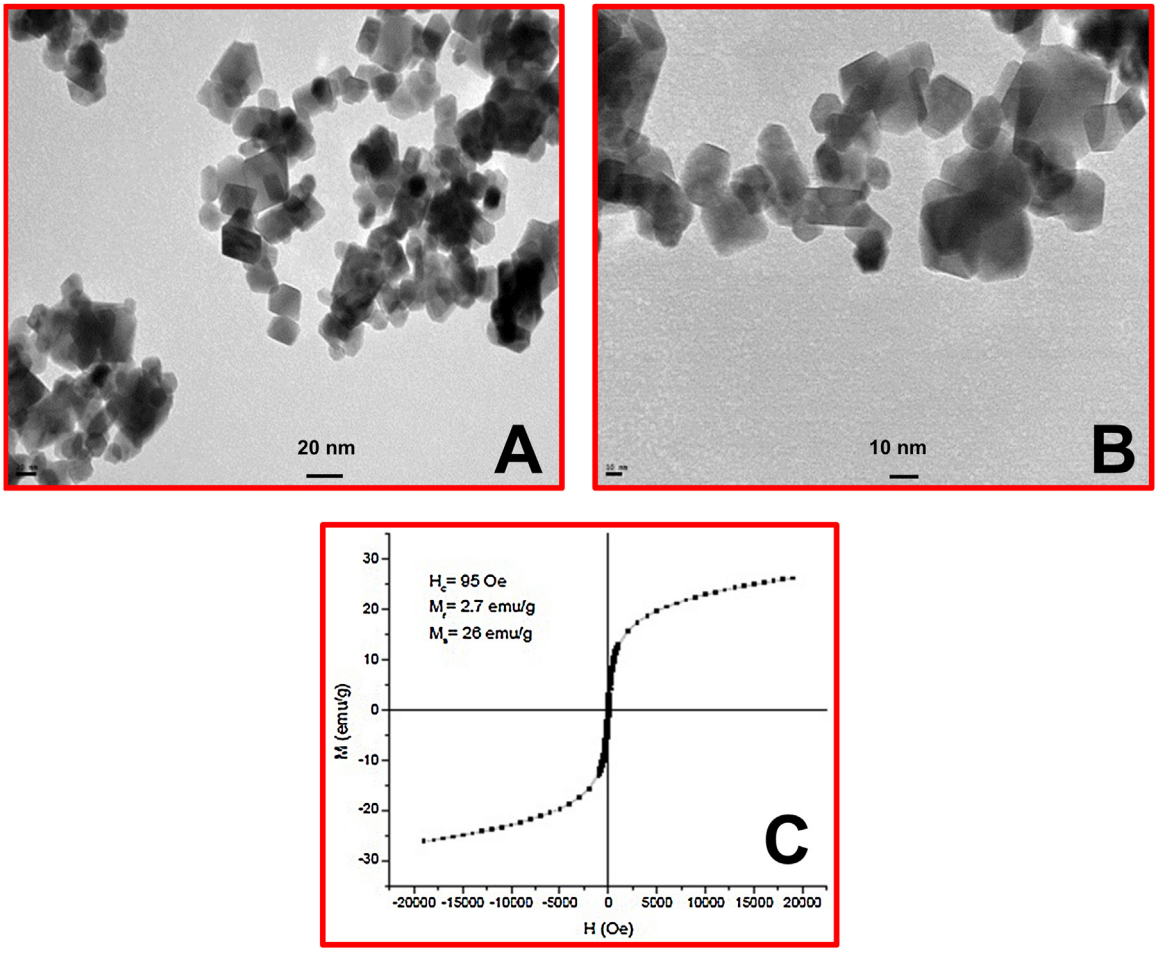

Fig. 2. Electronic micrographs of the calcined sample and magnetization study of the synthesized magnetic nanoparticles. (A) TEM: 270,000x; (B) TEM: 450,000 x and (C) hysteresis curve (20 °C) at maximum applied field of 1900 Oe.

Table 2
Comparison between NFNPs synthesized in the proposed work and those obtained from the literature.

Method	Ref. [33] Hydrothermal	Ref. [34] Hydrothermal	Ref. [35] Hydrothermal	Ref. [36] Co-precipitation	Ref. [37] Chemical combustion	This work Co-precipitation
Temperature of synthesis (°C)	200	150	200	80	80	Room temperature
Calcination (°C)	–	–	–	600–1000	600–800	600
Size						
Average diameter (nm)	10–20	10–60	15	8–28	17–35	16.6–20
Magnetic properties						
Ms (emu g^{-1})	58	35.1	52.2–60.8	40.5–45	26.6–36.9	26
Mr (emu g^{-1})	13.6	–	–	–	1.99–7.26	2.7
Hc (Oe)	166.7	–	–	89–175	56.1–104.6	95

structural water. For the calcined sample, the minimal weight loss observed can be associated to moisture evaporation (Fig. S3).

Table 2 shows a brief comparison between the NFNPs synthesized in the present work and those pointed out in the literature [33–37]. As can be seen, the proposed co-precipitation method allows obtaining NFNPs with a narrow distribution of size compared with the others co-precipitation and hydrothermal methods. On the other hand, high temperatures for synthesis are not required in this work. Additionally, the magnetic properties of the obtained NFNPs are comparable with those obtained employing other methods for synthesis.

3.2. Adsorption studies

3.2.1. Batch studies for adsorption of DIP on nickel ferrite

Fig. 3 shows adsorption kinetics and isotherms for calcined sample at pH 4 and 6 at 20 °C. Kinetic data show that the adsorption of DIP on NFNPs is relatively fast and reaches equilibrium after approximately 2 h of reaction. Generally, adsorption kinetic results were interpreted in the literature in terms of empirical equations, such as the pseudo-first order and the pseudo-second order kinetic equations, which are now known to be special cases of the Langmuir adsorption kinetics [38–40]. It is then more appropriate to use the Langmuir adsorption kinetics, for which a complete analytical solution has been found, and adsorption and desorption rate constants can be obtained. The analytical solution is called the Integrated Kinetic Langmuir equation, (IKL) [38] which is presented in Supplementary material. In Langmuir kinetics the overall adsorption rate ($d\theta/dt$) is defined as the difference in adsorption and desorption rates as follows:

$$\frac{d\theta}{dt} = v_a - v_d = k_a c(1-\theta) - k_d\theta \quad (2)$$

Where v_a is the adsorption rate, v_d the desorption rate, c the concentration and $\theta = a/a_m$ is the surface coverage at time t, being a and a_m the adsorbed amount at time t and the maximum adsorbed amount, respectively. k_a is the adsorption rate constant whereas k_d is the desorption rate constant. Under equilibrium conditions the adsorption and desorption rates are equal, the overall adsorption rate is zero, and thus Eq. (2) becomes the Langmuir isotherm:

$$\theta_{eq} = \frac{a_{eq}}{a_m} = Kc_{eq}/(1+Kc_{eq}) \quad (3)$$

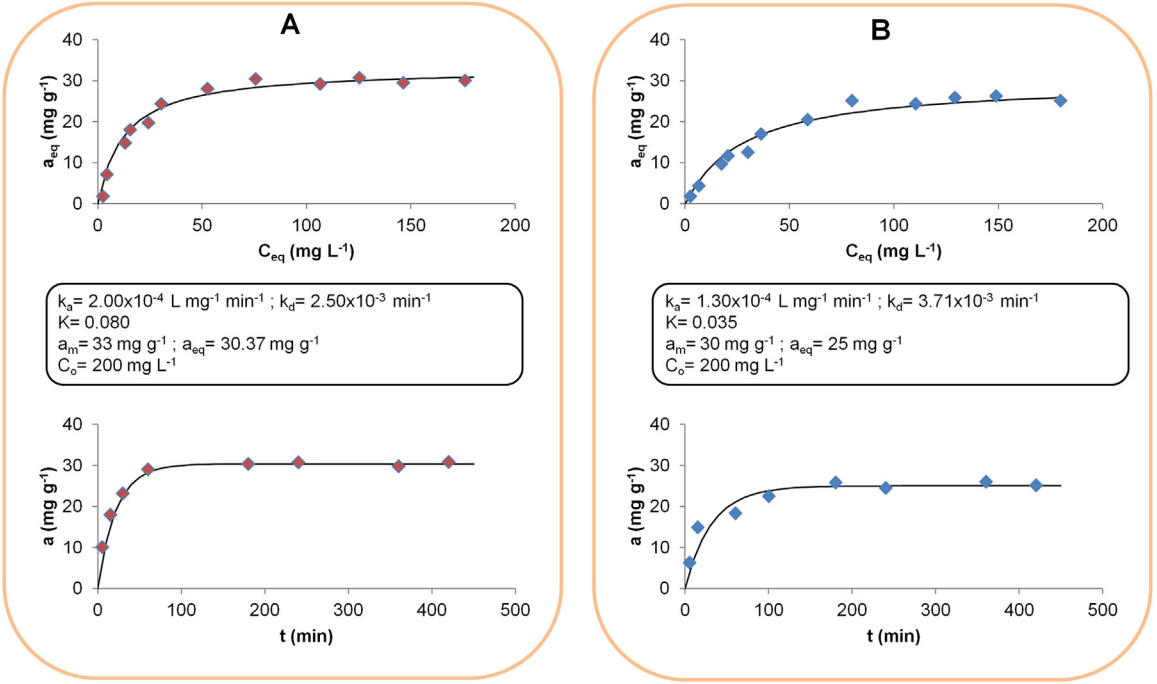

Fig. 3. Adsorption studies of DIP on NFNPs. (A) Kinetic and adsorption isotherms at pH 6.0, (B) Kinetics and adsorption isotherms at pH 4.0. Inset: parameters from IKL equation. Additional experimental details summarized in Section 3.2.1.

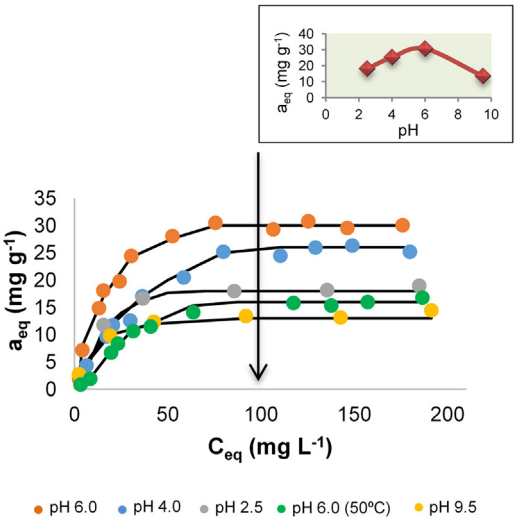

Fig. 4. Comparison of adsorption isotherms at different pH and temperature conditions. Inset: adsorbed DIP (mg g^{-1}) vs pH (Ceq: 100 mg L^{-1}, at 20 °C). Experimental conditions summarized in Section 3.2.1.

where θ_{eq} is the surface coverage at equilibrium and $K = k_a/k_d$ is the Langmuir constant. By using the IKL equation, adsorption kinetic curves (a vs t) can be fitted and the obtained k_a and k_d can be used to calculate K and to check this last value with the adsorption isotherm. An example for calculation is given in Supplementary material, and the results of such calculations are given as lines in Fig. 3. The equations worked very well, since at a given pH the same set of parameters produces a good fit of both, kinetic and equilibrium data. Indeed, k_a and k_d values that lead to a good fit of the kinetic curve generate the right K value to fit the adsorption isotherm. Calculations show that increasing the pH from 4 to 6 increases k_a and decreases k_d resulting in a higher overall adsorption rate and an increased adsorption under equilibrium.

Adsorption isotherms in the pH range 2.5–9.5 are shown in Fig. 4. Maximum adsorption occurred at pH 6 and both, acidic or basic conditions decreased DIP adsorption. Data are also compared to the adsorption isotherm at pH 6 and 50 °C. Results show that the maximum adsorption takes place at pH 6 and 20 °C. Increasing the temperature to 50 °C (keeping pH at 6) or changing the pH to 2.5 or 9.5 (keeping temperature at 20 °C) produce a rather similar decrease in the adsorption. Changes in temperature or pH, therefore, will be used below as possible strategies for desorption.

3.2.2. Effect of adsorbed DIP on the electrophoretic mobility of nickel ferrite

Results obtained by electrophoretic mobility measurements are shown in Fig. 5. The isoelectric point (IEP, pH where the electrophoretic mobility or the Zeta potential is zero) in NaCl solutions was 6.5, in agreement with IEP values previously reported in [41] and summarized by Kosmulski [42]. In the presence of DIP, the IEP shifted to around 5. Data show that DIP can change the charge of nickel ferrite from positive to negative in the pH range 5–6, proving that the interaction between the adsorbate and the surface is not purely electrostatic. The behavior is typical of specific adsorbing anions such as phosphate, arsenate and sulfate [43,44], which usually form surface complexes when adsorbing at the metal oxide-water interface (see Section 3.2.3).

3.2.3. Effect of ionic strength and co-existing ions

Typically, dissolved salts are present in water samples in a concentration range between 50 and 1000 mg L^{-1} for fresh water samples and between 1000 and 10000 mg L^{-1} for slightly and moderately saline water [45]. In order to evaluate the effect of ionic strength and the co-existing species on DIP adsorption several experiments were performed with different concentrations of NaCl, $NaHCO_3$, Na_2SO_4 and Na_2HPO_4 (10 mM to 200 mM). These salts were added to mixtures of DIP (100 mg L^{-1}) and 800 mg L^{-1} of NFNPs at pH 6.0 ± 0.2 and were mechanically shaken for 60 min to reach the equilibrium. As a result, the adsorption capacity decreased up to 48% when the concentration of the other salts increased (Fig. S4). This tendency was especially observed with phosphate and sulfate ions which strongly complex the surface of magnetic nanoparticles [46,47]. This behavior can be associated with the trend of DIP to form metallic complexes with M^{2+} and M^{3+} cations, as previously reported in the literature for reactions in aqueous media [48,49]. The fact that increasing the concentration of ligands such as phosphate or sulfate decreased DIP adsorption, and that adsorbed DIP produced an electrophoretic behavior typical of particles with specifically adsorbed anions suggests that the mechanism of DIP adsorption is formation of inner-sphere complexes with metal ions at the surface of the particles [42–44]. This is why good ligands are needed to desorb it.

3.3. Desorption studies

In order to evaluate the possible desorption of DIP from the adsorbent material a flow through system was designed for rinsing of NFNPs with minimal handling of samples and reagents (Fig. 6). In preliminary studies, basic and acidic solutions and polar organic solvents, such as methanol and ethanol, were tested as desorption

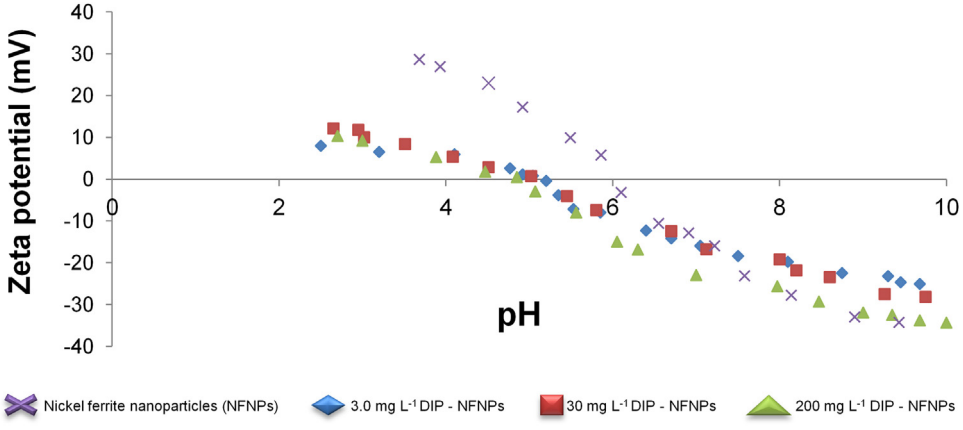

Fig. 5. Effect of adsorbed DIP on surface charge of nickel ferrite. Additional details in Section 3.2.2.

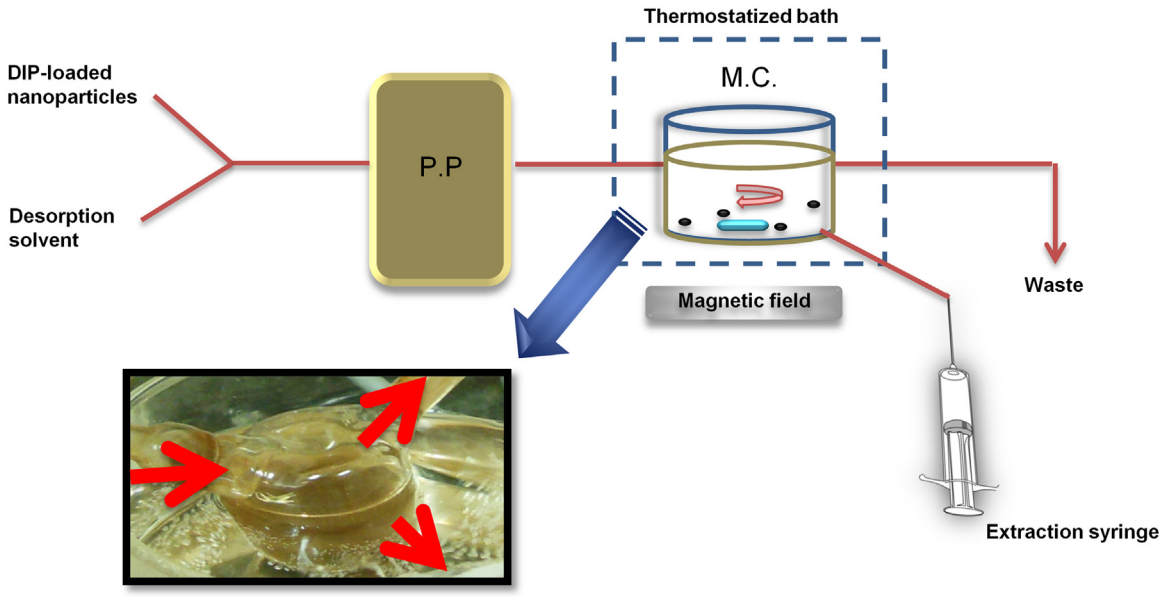

Fig. 6. Flow system for dynamic rinsing of NFNPs (P.P.: peristaltic pump; M.C.: mixing cell). Inset: mixing cell with the DIP-NFNPs aqueous mixture.

solvent. Due to the strong adsorption of DIP on NFNPs, the use of organic solvents was ineffective and only aqueous solutions at pH 2.5 or 9.5 (adjusted with 0.1 M HCl and 0.1 M NaOH, respectively) were useful to break the complex DIP-NFNPs. Since increasing temperature also decreased the adsorption, these aqueous solutions were evaluated for desorption at variable temperatures (25, 40, 60, 70 and 90 °C). Close to 20% of pre-sorbed amount of DIP was removed during the first 20 min at 25 °C, and the removal was increased to 40–45% at 50 °C, at both pH conditions (Fig. S5). Studies at higher temperatures were not successful as a consequence of DIP degradation, probably due to strong hydrolyzing conditions [50]. Taking this into account, an aqueous solution at pH 2.5 was chosen for evaluating the process by performing several extraction cycles at 50 °C. In this case, the flow system was implemented an each rinsing step was performed during 2 min followed by the magnetic recovery of the nanoparticles and quantification of the DIP in the supernatant as previously described (Section 2.5). From the obtained results, a 55% of desorption for DIP is achieved after six washing cycles performed at the selected temperature and under this strong acidic condition (Fig. 7).

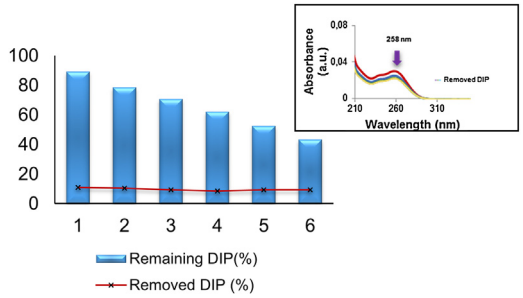

Fig. 7. Rinsing steps for desorption of DIP under strong acidic conditions (pH 2.5) at 50 °C. Experimental details in Section 3.3. Inset: UV–vis spectra recorded at 258 nm.

3.4. Evaluation of the adsorption performance of nickel ferrite nanoparticles

Due to the high polarity and high solubility of DIP in aqueous solution, the adsorptive removal of this compound and/or its metabolites has not been widely studied. Table 3 compares the DIP adsorption performance of the nickel ferrite investigated here with other materials. To the best of our knowledge, there are not research works in the literature where DIP is adsorbed onto metal oxides-based adsorbent including nickel ferrite. There is one report of DIP adsorption on chitosan spheres [51], but experiments were performed in ethanol and thus the results cannot be directly translated to DIP removal from water or to evaluate the performance of the adsorbent in decontamination of polluted waters. There is another report where DIP is extracted with an anionic exchange polymer in order to quantify it, but with only 36% adsorption [52]. Table 3 also includes adsorption data of different pharmaceutical compounds on magnetic materials [53–55]. Although some sorbents show satisfactory adsorption efficiency, most of them were used as hybrid materials or required appropriate functionalization of the surface prior to use. Hence, we demonstrate that the proposed $NiFe_2O_4$ can be used for removal of DIP from aqueous solution without any surface functionalization, requiring minimal volume of samples and sorbent material.

4. Conclusion

In this work nickel ferrite nanoparticles with a size of 20 ± 3 nm have been synthesized by a co-precipitation method at room temperature. The synthesized nanoparticles resulted polyhedral in shape with an IEP of 6.5 and ferromagnetic properties. Adsorption capacity of the synthesized nickel ferrite particles was tested for the removal of dipyrone as a model compound of polar emerging pollutant. The adsorption of DIP was found to be a pH and temperature dependent process and was successfully fitted by applying the IKL equation, which is the full solution of Langmuir adsorption kinetics. Due to the strong adsorption of DIP on NFNPs, the desorption process was only possible at low and high pH conditions and high temperatures. Additionally, this material

Table 3
Comparison of the adsorption of DIP on different solids, and of different pharmaceutical compounds on magnetic materials in the literature.

Adsorbent material	Pharmaceutical compounds	Experimental conditions for adsorption kinetics	Amount adsorbed at equilibrium (qe, mg g^{-1})	Ref.
Chitosan microspheres (*)	Dipyrone (DIP) Diclofenac (DIC)	$C_{adsorbent}$: 0.1 g L^{-1} Co: 2.0 g L^{-1} T: 25 °C Equilibrium contact time: 30 min	133 (DIP) 155 (DIC)	[51]
Mixed-mode reversed phase/anionic exchange Strata X-AW	Dipyrone	$C_{adsorbent}$: 200 mg/3 mL (commercial cartridge) T: 25 °C Sample volume: 500 mL	n.r.	[52]
Fe_3O_4	Chlorotetracycline	$C_{adsorbent}$: 0.05 g L^{-1} C_o: 5.0 mg L^{-1} T: 25 °C Sample volume: 50 mL pH: 6.5 Equilibrium contact time: 600 min	100	[53]
CNTs/$CoFe_2O_4$ composites	Sulfamethoxazole (SMX) 17β-estradiol (E2)	$C_{adsorbent}$: 0.1 g L^{-1} C_o: 2.0 mg L^{-1} T: 25 °C Sample volume:500 mL pH: 5.5 Equilibrium contact time: 120 min	6.98–7.43 (SMX) 19.3 – 20.0 (E2)	[54]
Thermal-responsive magnetic molecularly non-imprinted polymers (T-MNIPs) and Thermal-responsive magnetic molecularly imprinted polymers (T-MMIPs)	Norfloxacin	$C_{adsorbent}$: 1.3 g L^{-1} C_o: 80 mg L^{-1} T: 35 °C Sample volume: 6 mL Equilibrium contact time: 150 min	31.1 (T-MNIPs) 52.9 (T-MMIPs)	[55]
$NiFe_2O_4$	Dipyrone	$C_{adsorbent}$: 0.8 g L^{-1} C_o: 200 mg L^{-1} T: 20 °C Sample volume: 10 mL pH: 6.0 (4.0) Equilibrium contact time: 120 min	30.4 (pH 6.0) 25.0 (pH 4.0)	This work

n.r.: not reported, only 36% retention is informed in Supplementary material.
(*) in ethanol.

could be tested in a lab-scale flow through system due to its simple recovery using commercial Nd magnets. From the obtained results, the proposed nickel ferrite nanoparticles can be considered as alternative low-cost adsorbent for removal of polar pharmaceutical compounds from water samples.

Acknowledgements

The authors gratefully acknowledge financial support from SECyT-UNS and CONICET. E. Pecini and V. Springer also would like to express their gratitude to National Council of Scientific and Technical Research (CONICET) for the doctoral and post-doctoral fellowships. M.A is member of CONICET.

Appendix A. Supplementary data

Supplementary data associated with this article can be found, in the online version, at http://dx.doi.org/10.1016/j.jece.2016.08.026.

References

[1] M. La Farré, S. Pérez, L. Kantiani, D. Barcelo, Fate and toxicity of emerging pollutants, their metabolites and transformation products in the aquatic environment, TrAC Trends Anal. Chem. 27 (2008) 991–1007.
[2] A.A. Bletsou, J. Jeon, J. Hollender, E. Archontaki, N.S. Thomaidis, Targeted and non-targeted liquid chromatography-mass spectrometric workflows for identification of transformation products of emerging pollutants in the aquatic environment, Trends Anal. Chem. 66 (2015) 32–44.
[3] World Health Organization, WHO/HSE/WSH/11.05 report, Pharmaceuticals in Drinking water. http://www.who.int/water_sanitation_health/publications/2011/pharmaceuticals_20110601.pdf, 2011 (accessed 11.08.16).
[4] B.D. Blair, J.P. Crago, C.J. Hedman, R.D. Klaper, Pharmaceuticals and personal care products found in the Great Lakes above concentrations of environmental, Chemosphere 93 (2013) 2116–2123.
[5] K. Hedenmalm, O. Spigset, Agranulocytosis and other blood dyscrasias associated with dipyrone (metamizole), Eur. J. Clin. Pharmacol. 58 (2002) 265–274.
[6] D.F. Feldmann, S. Zuehlke, T. Hebere, Occurrence, fate and assessment of polar metamizole (dipyrone) residues in hospital and municipal wastewater, Chemosphere 71 (2008) 1754–1764.
[7] EMEA/MRL/878/03, Committee for veterinary medicinal products, Metamizole (2003) http://www.ema.europa.eu/docs/en_GB/document_library/Maximum_Residue_Limits_-_Report/2009/11/WC500015055.pdf, (accessed 11.08.16).
[8] M. Kostopoulou, A. Nikolaou, Analytical problems and the need for sample preparation in the determination of pharmaceuticals and their metabolites in aqueous environmental matrices, Trends Anal. Chem. 27 (2008) 1023–1035.
[9] S. Yuan, X. Jiang, X. Xia, H. Zhang, S. Zheng, Detection, occurrence and fate of 22 psychiatric pharmaceuticals in psychiatric hospital and municipal wastewater treatment plants in Beijing, China, Chemosphere 90 (2013) 2520–2525.
[10] H.R. Rajabi, H. Arjmand, S.J. Hoseini, H. Nasrabadi, Surface modified magnetic nanoparticles as efficient and green sorbents: synthesis, characterization and application for the removal of anionic dye, J. Magn. Magn. Mater. 394 (2015) 7–13.
[11] M.C. Mascolo, Y. Pei, T.A. Ring, Room temperature co-precipitation synthesis of magnetite nanoparticles in a large pH window with different bases, Materials 6 (2013) 5549–5567.
[12] P. Pulišová, J. Kováč, A. Voigt, P. Raschman, Structure and magnetic properties of Co and Ni nano-ferrites prepared by a two-step direct microemulsions synthesis, J. Magn. Magn. Mater. 341 (2013) 93–99.
[13] R.B. Kamble, V.L. Mathe, Nanocrystalline nickel ferrite thick film as an efficient gas sensor at room temperature, Sens. Actuators B Chem. 131 (2008) 205–209.
[14] Y. Fu, H. Chen, X. Sun, X. Wang, Graphene-supported nickel ferrite: a magnetically separable photocatalyst with high activity under visible light, AIChE J. 58 (2012) 3298–3305.
[15] H.R. Rajabi, H. Arjmand, H. Kazemdehdashti, M. Farsi, A comparison investigation on photocatalytic activity performance and adsorption efficiency for the removal of cationic dye: quantum dots vs. magnetic nanoparticles, J. Environ. Chem. Eng. 4 (2016) 2830–2840.

[16] Q. Zhou, Z. Li, C. Shuang, A. Li, M. Zhang, M. Wang, Efficient removal of tetracycline by reusable magnetic microspheres with a high surface area, Chem. Eng. J. 210 (2012) 350–356.
[17] L. Sun, L. Chen, X. Sun, X. Du, Y. Yue, D. He, H.X.Q. Zeng, H. Wang, L. Ding, Analysis of sulfonamides in environmental water samples based on magnetic mixed hemimicelles solid-phase extraction coupled with HPLC–UV detection, Chemosphere 77 (2009) 1306–1312.
[18] A. Afkhami, S. Razieh Moosavi, T. Madrakian, Magnetic nickel zinc ferrite nanocomposite as an efficient adsorbent for the removal of organic dyes from aqueous solutions, J. Ind. Eng. Chem. 21 (2015) 920–924.
[19] L. Zhang, X. Liu, X. Guo, M. Su, T. Xu, X. Song, Investigation on the degradation of brilliant green induced oxidation by $NiFe_2O_4$ under microwave irradiation, Chem. Eng. J. 173 (2011) 737–742.
[20] P. Leroy, C. Tournassat, M. Bizi, Influence of surface conductivity on the apparent zeta potential of TiO_2 nanoparticles, J. Colloid Interface Sci. 356 (2011) 442–453.
[21] http://www.chemicalize.org (accessed 04.08.16).
[22] L.H. Marcolino Jr., R.A. Sousa, O. Fatibello-Filho, F.C. Moraes, M.F.S. Teixeira, Flow-injection spectrophotometric determination of dipyrone in pharmaceutical formulations using ammonium molybdate as chromogenic reagent, Anal. Lett. 38 (2005) 2315–2326.
[23] I. Quino, R. Choque, L.F. Cáceres, Validación de una nueva determinación espectrofotométrica para dipirona en fármacos, Rev. Bol. Quim. 22 (2005) 64–70.
[24] C.L. Huang, E. Matijevic, Preparation and characterization of ultrafine iron-rich nickel ferrites, Solid State Ionics 84 (1996) 249–258.
[25] H.P. Klug, L.E. Alexander, X-ray Diffraction Procedures for Polycrystalline and Amorphous Materials, second ed., Wiley, New York, 1974.
[26] S.K. Kurinec, N. Okeke, S.K. Gupta, H. Zhang, T.D. Xiao, Synthesis and electrophoretic deposition of magnetic nickel ferrite nanoparticles, J. Mater. Sci. 41 (2006) 8181–8185.
[27] S. Gunasekaran, G. Anbalagan, S. Pandi, Raman and infrared spectra of carbonates of calcite structure, J. Raman Spectrosc. 37 (2006) 892–899.
[28] S. Joshi, M. Kumar, S. Chhoker, G. Srivastava, M. Jewariya, V.N. Singh, Structural magnetic, dielectric and optical properties of nickel ferrite nanoparticles synthesized by co-precipitation method, J. Mol. Struct. 1076 (2014) 55–62.
[29] S. Music, S. Popovic, S. Dalipi, Formation of oxide phases in the system Fe_2O_3-NiO, J. Mater. Sci. 28 (1993) 1793–1798.
[30] M.P. Morales, S. Veintemillas-Verdaguer, M.I. Montero, C.J. Serna, Surface and internal spin canting in γ-Fe_2O_3 nanoparticles, Chem. Mater. 11 (1999) 3058–3064.
[31] A.W. Burton, K. Ong, T. Rea, I.Y. Chan, On the estimation of average crystallite size of zeolites from the Scherrer equation: a critical evaluation of its application to zeolites with one-dimensional pore systems, Microporous Mesoporous Mat. 117 (2009) 74–90.
[32] A. Goldman, Modern Ferrites Technology, second ed., Springer, New York, 2006.
[33] L. Wang, J. Li, Y. Wang, L. Zhao, Q. Jiang, Adsorption capability for congo red on nanocrystalline MFe_2O_4 (M = Mn Fe, Co, Ni) spinel ferrites, Chem. Eng. J. 181-182 (2012) 72–79.
[34] K. Nejati, R. Zabihi, Preparation and magnetic properties of nano size nickel ferrite particles using hydrothermal method, Chem. Cent. J. 6 (2012) 23–29.
[35] L.S. Fu, C.Y. Xu, W.S. Wang, J.T. Jiang, L. Zhen, Superparamagnetic nickel ferrite colloidal spheres for constructing magnetically responsive photonic crystals, Mater. Lett. 81 (2012) 62–64.
[36] K. Maaz, S. Karim, A. Mumtaz, S.K. Hasanain, J. Liu, J.L. Duan, Synthesis and magnetic characterization of nickel ferrite nanoparticles prepared by co-precipitation route, J. Magn. Magn. Mater. 321 (2009) 1838–1842.
[37] T. Shanmugavel, S. Gokul Raj, G. Ramesh Kumar, G. Rajarajan, D. Saravanan, Cost effective preparation and characterization of nanocrystalline nickel ferrites ($NiFe_2O_4$) in low temperature regime, J. King. Saud. Univ. Sci. 27 (2015) 176–181.
[38] A.W. Marczewski, Analysis of kinetic langmuir model. Part I: integrated kinetic langmuir equation (IKL): a new complete analytical solution of the langmuir rate equation, Langmuir 26 (2010) 15229–15238.
[39] S. Azizian, Kinetic models of sorption: a theoretical analysis, J. Colloid Interface Sci. 276 (2004) 47–52.
[40] Y. Liu, L. Shen, From langmuir kinetics to first- and second-order rate equations for adsorption, Langmuir 24 (2008) 11625–11630.
[41] R.C. Plaza, J. de Vicente, S. Gomez-Lopera, A.V. Delgado, Stability of dispersions of colloidal nickel ferrite spheres, J. Colloid Interface Sci. 242 (2001) 306–313.
[42] M. Kosmulski, IEP as a parameter characterizing the pH-dependent surface charging of materials other than metal oxides, Adv. Colloid. Interface Sci. 171–172 (2012) 77–86.
[43] T. Hiemstra, W.H. Van Riemsdijk, A surface structural approach to ion adsorption: the charge distribution (CD) model, J. Colloid Interface Sci. 179 (1996) 488–508.
[44] J. Antelo, M. Avena, S. Fiol, R. López, F. Arce, Effects of pH and ionic strength on the adsorption of phosphate and arsenate at the goethite-water interface, J. Colloid Interface Sci. 285 (2005) 476–486.
[45] U.S Geological Survey, http://water.usgs.gov/edu/saline.html (accessed 05.05.16).
[46] T.J. Daou, S. Begin-Colin, J.M. Greneche, F. Thomas, A. Derory, P. Bernhardt, P. Legaré, G. Pourroy, Phosphate adsorption properties of magnetite-based nanoparticles, Chem. Mater. 19 (2007) 4494–4505.
[47] C. Mansour, G. Lefèvre, E.M. Pavageau, H. Catalette, M. Fédoroff, S. Zanna, Sorption of sulfate ions onto magnetite, J. Colloid Interface Sci. 331 (2009) 77–82.
[48] W.T. Suarez, O.D. Pessoa-Neto, F.C. Vicentini, B.C. Janegitz, R.C. Faria, O. Fatibello-Filho, Flow injection spectrophotometric determination of dipyrone in pharmaceutical formulations using Fe(III) as reagent, Anal. Lett. 44 (2011) 340–348.
[49] V.G. Bonifácio, O. Fatibello-Filho, L.H. Marcolino-Júnior, Flow-injection spectrophotometric determination of dipyrone in pharmaceutical formulations using a solid-phase reactor with copper(II) phosphate, Cent. Eur. J. Chem. 11 (2013) 1830–1836.
[50] H. Ergün, D.A.C. Frattarelli, J.V. Aranda, Characterization of the role of physicochemical factors on the hydrolysis of dipyrone, J. Pharm. Biomed. Anal. 35 (2004) 479–487.
[51] T.O. Carvalho, A.E.B. Matias, L.R. Braga, S.M. Evangelista, A.G.S. Prado, Calorimetric studies of removal of nonsteroidal anti-inflammatory drugs diclofenac and dipyrone from water, J. Therm. Anal. Calorim. 106 (2011) 475–481.
[52] P. Paíga, A. Lolić, F. Hellebuyck, L.H.M.L.M. Santos, M. Correia, C. Delerue-Matos, Development of a SPE-UHPLC-MS/MS methodology for the determination of non-steroidal anti-inflammatory and analgesic pharmaceuticals in seawater, J. Pharm. Biomed. Anal. 106 (2015) 61–70.
[53] D. Zhang, H. Niu, X. Zhang, Z. Meng, Y. Cai, Strong adsorption of chlorotetracycline on magnetite nanoparticles, J. Hazard. Mater. 192 (2011) 1088–1093.
[54] F. Wang, W. Sun, W. Pan, N. Xu, Adsorption of sulfamethoxazole and 17β-estradiol by carbon nanotubes/CoFe2O4 composites, Chem. Eng. J. 274 (2015) 17–29.
[55] W. Huang, Y. Kong, W. Yang, X. Ni, N. Wang, Y. Lu, W. Xu, Preparation and characterization of novel thermosensitive magnetic molecularly imprinted polymers for selective recognition of norfloxacin, J. Polym. Res. 23 (2016), doi: http://dx.doi.org/10.1007/s10965-016-0972-y.